

5630

This report is a preprint of an article submitted to a journal for publication. Because of changes that may be made before formal publication, this preprint is made available with the understanding that it will not be cited or reproduced without the permission of the author.

## Thermodynamic Assessment of the $Y_2O_3$ - $Yb_2O_3$ - $ZrO_2$ System

Nathan S. Jacobson  
NASA Glenn Research Center  
Cleveland, OH 44135

Zi-Kui Liu  
Department of Materials Science and Engineering  
Pennsylvania State University  
State College, PA 16802

Larry Kaufman  
Brookline, MA 02146

Fan Zhang  
Computherm LLC  
Madison, WI 53719

### Introduction

The rare earth oxide-zirconia systems are used for a variety of applications, such as solid electrolytes and thermal barrier coatings. To gain a better insight into their behavior and further improve their performance, it is essential to understand the thermodynamic properties of these materials. These thermodynamic properties dictate the stability of the oxides in actual service conditions. Today thermodynamics involves both experimental measurements and development of self-consistent databases which contain the Gibbs energies of the individual phases (1). Parameters in various solution models are evaluated based on available experimental data. From a set of relatively simple equations, all phase boundaries and thermodynamic properties can be calculated for a particular system through minimization of the Gibbs energy under given conditions. Further, binary systems are building blocks for higher order systems, which may not be experimentally studied.

Yttria-zirconia ( $Y_2O_3$ - $ZrO_2$ ) is the most widely used of the rare earth oxide-zirconia systems. There are numerous experimental studies of the phase boundaries in this system. In this paper, we assess these data and derive parameters for the solution models in this system. There is current interest in other rare earth oxide-zirconia systems as well as systems with several rare earth oxides and zirconia, which may offer improved properties over the  $Y_2O_3$ - $ZrO_2$  system. For this reason, we also assess the ytterbia-zirconia ( $Yb_2O_3$ - $ZrO_2$ ) and  $Y_2O_3$ - $Yb_2O_3$ - $ZrO_2$  system. Only limited experimental data are currently available for the  $Yb_2O_3$ - $ZrO_2$  binary and  $Y_2O_3$ - $Yb_2O_3$ - $ZrO_2$  ternary systems.

There are several calculations of the  $Y_2O_3$ - $ZrO_2$  system in the literature. Kaufman (2) approaches this type of pseudo-binary by treating each oxide unit (i.e.  $Y_2O_3$  and  $ZrO_2$ ) as a component. This readily allows development of quite good oxide databases with a minimum number of components. The experimental phase diagram for  $Y_2O_3$ - $ZrO_2$  is

dominated by a large cubic phase field for  $\text{ZrO}_2$  as well as a large cubic phase field for  $\text{Y}_2\text{O}_3$ . Degtyarev and Voronin (3,4) point out that the cubic  $\text{Y}_2\text{O}_3$  phase can be derived from the  $\text{ZrO}_2$  phase by removing two oxygen anions. Thus they treat the two cubic phases as one cubic phase with a miscibility gap. Du et al. (5,6) model the  $\text{Y}_2\text{O}_3$ - $\text{ZrO}_2$  system using the miscibility gap simplification and treating  $\text{YO}_{1.5}$  and  $\text{ZrO}_2$  as components. They do a thorough literature survey and derive their model coefficients using experimental data (7). They do not consider experimental data below  $\sim 1300$  K, due to likely difficulties in attaining equilibria. One of their assessments uses the liquid as the reference state (5) and the other uses the standard element reference state (6). Yokokawa et al. (8,9) calculate the  $\text{Y}_2\text{O}_3$ - $\text{ZrO}_2$  diagram and phase diagrams for a number of other rare earth oxide-zirconia systems. They also treat the oxide units as components and derive solution parameters from both phase boundary data and correlations between ionic radii of metal oxides.

No calculations were found for any ternaries or higher order systems. In this study we assess the  $\text{Y}_2\text{O}_3$ - $\text{ZrO}_2$ ,  $\text{Yb}_2\text{O}_3$ - $\text{ZrO}_2$ , and  $\text{Y}_2\text{O}_3$ - $\text{Yb}_2\text{O}_3$  binaries from available data. We re-assess the  $\text{Y}_2\text{O}_3$ - $\text{ZrO}_2$  for two reasons—to build a database without the miscibility gap simplification and to include more low temperature data. We do not use the miscibility gap simplification for two reasons. First, the space groups of cubic  $\text{Y}_2\text{O}_3$  and cubic  $\text{ZrO}_2$  are not the same. Second, the use of separate phases makes convergence easier. The oxide units  $\text{Y}_2\text{O}_3$ ,  $\text{Yb}_2\text{O}_3$ , and  $\text{ZrO}_2$  are used as components. The model parameters are derived from experimental data. Then these three binary assessments are combined to form the ternary  $\text{Y}_2\text{O}_3$ - $\text{Yb}_2\text{O}_3$ - $\text{ZrO}_2$  database.

## Review of Experimental Data

### Pure Components and Lattice Stabilities

All data is in the form of Gibbs energies with the standard element reference state (SER). Transition heats and temperatures are given in Table I(a). These data are from the STGE database (10), which in turn were taken from IVTAN database (11). Adjustments are made to the transition temperatures of  $\text{Y}_2\text{O}_3$  in order to maintain consistency with the  $\text{Y}_2\text{O}_3$ -rich data of Stubican et al. (12), which is the most complete dataset for the  $\text{Y}_2\text{O}_3$ -rich side of the diagram. Further the IVTAN heat of transition between the two solid phases is 54 kJ/mol, which is rather high. A more reasonable estimate for a solid oxide/solid oxide transformation is 20 kJ/mol (13) and this is used in the database.

The SGTE and IVTAN data for  $\text{Yb}_2\text{O}_3$  are incomplete. The SGTE database lists only one solid phase for  $\text{Yb}_2\text{O}_3$ , whereas the IVTAN tables list two solid phases, but with no heat of transition between the two solid phases. In analogy with  $\text{Y}_2\text{O}_3$ , the lower temperature solid phase is taken as cubic and the high temperature solid phase as hexagonal and the heat of transition is estimated to be 20 kJ/mol. The transition temperatures are taken from IVTAN (11).

Solution database development is based on the determination of lattice stabilities (1). For the pure elements, these have been determined and tabulated. However, when using oxide units as components, these must be estimated. Lattice stabilities are chosen to make the particular phase unstable over the entire range by adding  $\sim 20$  kJ/mol to the

stable phase's Gibbs energy for a given temperature range. All lattice stabilities are listed in Table II(b).

### **Y<sub>2</sub>O<sub>3</sub>-ZrO<sub>2</sub> System—Phase Boundary Data**

There is a good deal of experimental phase boundary information on this system (12,14-38). The data through 1990 are reviewed by Du et al. (5,6). Figure 1(a) and (b) show two accepted experimental phase diagrams (14,15). Both diagrams are dominated by a large cubic ZrO<sub>2</sub> phase field. Both diagrams contain several invariant points, which are listed in Table II. The differences between the two experimental diagrams indicate the many controversies in this diagram. Du et al. (5,6) state that the difficulty in attaining low temperature equilibria make the low temperature eutectoids unreliable. Therefore they do not use them in their assessment. The Y<sub>2</sub>O<sub>3</sub>-ZrO<sub>2</sub> system can be viewed as a rigid cation lattice with mobile anions. Due to the low diffusivity of the cations, phase changes are very slow, particularly at the lower temperatures. This fact must be considered in assessing experimental data. In the following discussion we examine available experimental data paying particular attention to the technique and reliability of the data.

There are three measurements of the liquidus line (17-19). Skaggs (19) used a laser heating method to create a 'pendant drop'. Temperature measurements were taken with a small amount of solid in the drop and then again with approximately half the drop solid. The average of these gave the liquidus temperature. However, these data showed a large amount of scatter and are not used in this assessment. Noguchi et al. (17) used a solar furnace in conjunction with a pyrometer. Cooling curves clearly revealed the solidification point. Rouanet (18) has used a similar technique and his data are in basic agreement with Noguchi et al. (17). The data of Noguchi et al. (17) are thus used in this assessment.

The ZrO<sub>2</sub>-rich side of the diagram is the area of the greatest practical interest. As noted, the equilibrium phases of ZrO<sub>2</sub> are monoclinic, tetragonal, and cubic as temperature increases. In addition, quenched samples also form a persistent, non-equilibrium tetragonal phase (32). The non-equilibrium tetragonal phase has a smaller c axis and generally higher Y<sub>2</sub>O<sub>3</sub> contents than the corresponding equilibrium tetragonal phase (37). Some of the discrepancies in reported experimental data are likely due to the formation of this metastable phase (32, 37).

The most well-known transformation of ZrO<sub>2</sub> is the monoclinic to tetragonal transformation, which is accompanied by a 3-5% volume increase. Four measurements were found of this transformation (16, 24, 27, 31)—all show that the transformation temperature decreases with increasing Y<sub>2</sub>O<sub>3</sub> content. Duwez et al. (16) observed a sharp change in expansion on the tetragonal to monoclinic transformation. Pascual and Duran (24) used dilatometry and differential thermal analysis (DTA). Ruh et al. (27) used XRD and Yoshikawa and Suto (31) used dilatometry. In the mole fraction of Y<sub>2</sub>O<sub>3</sub> from 0.00 to 0.02, these data all show reasonably good agreement. However, Duwez et al. (16) and Pascual and Duran (24) show the transformation temperature continues to decrease to a mole fraction of Y<sub>2</sub>O<sub>3</sub> ~ 0.05. Only the mole fraction of Y<sub>2</sub>O<sub>3</sub> from 0.00 to 0.02 data are used in this assessment.

There are the most data for cubic/tetragonal equilibria at the  $\text{ZrO}_2$ -rich side (12, 16, 21, 23-25, 30, 36, 38). Duwez et al. (16) used XRD to determine the cubic/(cubic + tetragonal) boundaries at 1648 and 2273 K. Ruh et al. (27), Pascual and Duran (24), Scott (21) and Stubican et al. (12) have taken similar measurements with XRD. Ruhle et al. (25) and Lanteri et al. (23) used analytical electron microscopy to determine the tetragonal/(tetragonal + cubic)/cubic phase boundaries. Their data indicates these boundaries are temperature independent. Yoshikawa et al. (30) used electron microprobe analysis to determine these phase boundaries. The data points for all these investigations are collected in Figure 2 and show remarkably good agreement with each other at temperatures greater than  $\sim 1600$  K. At lower temperatures the mole fraction of  $\text{Y}_2\text{O}_3$  differs by  $\sim 0.02$ .

The cubic phase field on the  $\text{ZrO}_2$ -rich side occupies a large section of the diagram and extends to low temperatures (33). Stubican et al. (12) has proposed a low temperature eutectoid, as noted in Table II, which is included in this assessment.

There is one confirmed intermediate compound in this system— $\text{Y}_3\text{Zr}_4\text{O}_{12}$  (12). This is an ordered phase, which decomposes to the disordered cubic solution. As shown in Table II, there is some controversy of its decomposition temperature. Other investigators have reported a pyrochlore-type compound of the form  $\text{Zr}_2\text{Y}_2\text{O}_7$  (24). However the existence of this compound is controversial—many investigators have not observed it, despite careful studies to search for it (34). Therefore it is not considered in this assessment.

As shown in the experimental phase diagram (Figure 1(a) and (b)), there are large cubic  $\text{ZrO}_2$  and cubic  $\text{Y}_2\text{O}_3$  regions, as well as a two phase region. Stubican et al. (12) have determined the phase boundaries of both sides of this two phase field by XRD. Pascual and Duran (24) have also used XRD to determine the cubic  $\text{ZrO}_2$ /(cubic  $\text{ZrO}_2$  + cubic  $\text{Y}_2\text{O}_3$ ) boundary. Their data is a mole fraction of  $\text{Y}_2\text{O}_3$   $\sim 0.08$  higher than that of Stubican et al. (12). Jayaratna et al. (36) have also measured these boundaries. Their data for the cubic  $\text{ZrO}_2$ /(cubic  $\text{ZrO}_2$  + cubic  $\text{Y}_2\text{O}_3$ ) boundary shows excellent agreement with that of Stubican et al. (12). The data of Stubican et al. (12) is used in this assessment.

Finally, the  $\text{Y}_2\text{O}_3$ -rich side of the diagram is less well studied. It is dominated by the cubic  $\text{Y}_2\text{O}_3$  phase, which transforms to the hexagonal  $\text{Y}_2\text{O}_3$  phase at high temperatures. The liquidus data in this region and the phase boundary data is given by Stubican et al. (12). Again, this data is the most complete for this side. As noted, some corrections were made to the  $\text{Y}_2\text{O}_3$  lattice stabilities for consistency with these data.

### **$\text{Y}_2\text{O}_3$ - $\text{ZrO}_2$ System—Thermodynamic Data**

There is only limited thermodynamic data on this system. Belov and Semenov (39) have measured the activity of  $\text{ZrO}_2$  and  $\text{Y}_2\text{O}_3$  at 2773 K using a Knudsen cell vapor pressure measurement technique. There are some inconsistencies between these data and the reported cubic/liquid phase boundary as shown in Figure 3. Assuming a pseudo-binary, there should be a constant activity in the (liquid + cubic) two phase region. There are two possible reasons for this inconsistency—either the temperature measurement is off or since the system is not truly a binary, but rather a Y-Zr-O ternary,  $P(\text{O}_2)$  is varying in the

experiment. Following Du et al. (4), we only include the first three  $ZrO_2$ -rich measurements in this assessment.

One calorimetric measurement was found for the heat of formation of an intermediate compound of the formula  $Zr_2Y_2O_7$  (40) and is given in Table III. However a compound of this stoichiometry has not been observed experimentally. First principles calculations are available for the heat of formation of  $Zr_3Y_4O_{12}$  (41) and are also listed in Table III.

### **$Yb_2O_3$ - $ZrO_2$ System—Phase Boundary Data**

There is much less experimental data available on this system and only phase boundary information was found. Only one liquidus measurement was found (18). The  $ZrO_2$ -rich side of the at temperatures below the solidus line has been studied by Corman (26, 29). It is similar to the  $ZrO_2$ -rich side of the  $Y_2O_3$ - $ZrO_2$  phase diagram and also contains an intermediate compound  $Zr_3Yb_4O_{12}$ , which disorders at a higher temperature than  $Zr_3Y_4O_{12}$  as listed in Table II.

### **$Y_2O_3$ - $Yb_2O_3$ - $ZrO_2$ System**

The  $Y_2O_3$ - $Yb_2O_3$ - $ZrO_2$  system appears to be the only pseudo-ternary system with  $ZrO_2$  and two rare-earth oxides, which has been experimentally studied. Corman (26) and Corman and Stubican (29) have examined this system at three temperatures from pure  $ZrO_2$  to solutions with a mole fraction of  $Y_2O_3$  equal to 0.5 and a mole fraction of  $Yb_2O_3$  equal to 0.5. Their diagrams at 1473, 1673, and 1923 K are shown in Figures 4(a), (b), (c), respectively.

The ternaries are characterized by continuous tetragonal  $ZrO_2$ , cubic  $ZrO_2$ , and cubic  $(Y,Yb)_2O_3$  solutions. Further the intermediate line compound,  $Zr_3(Y,Yb)_4O_{12}$ , extends across the diagram when both ends are stable (Figure 4(a)). As temperature is raised above 1655 K, the  $Zr_3Y_4O_{12}$  side disappears (Figure 4(b)). Above 1910 K, the compound disappears entirely (Figure 4(c)).

### **Modeling**

As discussed, the oxide units are treated as components. The lattice stabilities are listed in Table I(b).

Each of the solutions are modeled with random mixing term and a Redlich-Kister polynomial (42) to describe the excess free energy:

$$G_m(x, T) = \sum_{i=1}^2 x_i {}^\circ G_i(T) + RT \sum_{i=1}^2 x_i \ln x_i + {}^{ex}G_m \quad (1)$$

$${}^{ex}G_m = x_1 x_2 \sum_{j=0}^n {}^jL(x_1 - x_2)^j \quad (2)$$

Here  $x_i$  is the mole fraction of component  $i$ ,  ${}^\circ G_i(T)$  is the lattice stability of that component (Table I(b)),  ${}^jL$  are the interaction parameters,  $R$  is the gas constant, and  $T$  is

the absolute temperature. In this assessment, only the first two terms of the Redlich-Kister polynomials were used:

These interaction parameters were evaluated from the experimental data via the optimizing code Parrot in ThermoCalc\* and also the optimizing code in WinPhad\*\*. First the  $Y_2O_3$ - $ZrO_2$  diagram was obtained by fitting the liquidus and the approximate boundaries of the large cubic phase fields. The smaller phase regions were added by fine-tuning the parameters. A number of optimizations from different starting points were done to get the best fit with no artifacts. The  $Yb_2O_3$ - $ZrO_2$  diagram was done by using the parameters from the  $Y_2O_3$ - $ZrO_2$  system and making adjustments for the differences in the two systems.

ThermoCalc uses the Muggianu approach (43) to extend the binaries to ternaries. This approach gives the correct limits when the ternary solutions reduce to the binaries. In addition a ternary interaction parameter was added of the form:

$${}^{\text{ex-tern}}G_m = x_1x_2x_3{}^{\circ}L(\text{tern}) \quad (4)$$

These parameters were determined by 'trial and error' to get the best agreement with the experimental ternary sections.

## Results and Discussion

The solution parameters for the  $Y_2O_3$ - $ZrO_2$  system and are shown in Table IV. In most cases the  ${}^0L$  and  ${}^1L$  parameters are needed; however in some cases only the  ${}^0L$  parameter is needed. The complete calculated phase diagram is shown in Figure 5(a) with experimental data shown as symbols. Nearly all features of the experimental diagram (Figure 1(a) and (b)) are reproduced including the five invariant points (Table II), the liquidus lines, and the cubic  $ZrO_2$ /(cubic  $ZrO_2$  + cubic  $Y_2O_3$ )/cubic  $Y_2O_3$  phase boundaries. Only the tetragonal  $ZrO_2$ /(tetragonal  $ZrO_2$  + cubic  $ZrO_2$ )/cubic  $ZrO_2$  does not follow the experimentally measured phase boundaries, as shown in Figure 5(b). The highest temperature points are reproduced, but the calculated diagram does not reproduce the measured lack of temperature dependence of these boundaries. The appearance of the monoclinic solid solution at 1445 K also pushes these boundaries into higher  $Y_2O_3$  contents.

Figure 6 shows the calculated activities in this pseudo-binary at 2773 K. Note the two phase (liquid + cubic  $ZrO_2$ ) region with constant activity. The experimental data are shown as data points. The measured activity of  $ZrO_2$  was used in the assessment and shows very good agreement. The activity of  $Y_2O_3$  was not used and shows approximate agreement with the calculations.

The enthalpy of formation for  $Zr_3Y_4O_{12}$  is also extracted from this assessment from:



\* ThermoCalc Ver. N, ThermoCalc Software, Stockholm, Sweden

\*\* WinPhad Pro 2.0, Computherm LLC, Madison, WI.

The value from the assessment (-45.9 kJ/mol) shows order of magnitude agreement with the calculations from first principles (Table III, ref. (41)).

The parameters for the  $\text{Yb}_2\text{O}_3\text{-ZrO}_2$  system are given in Table V and the calculated phase diagram is given in Figure 7. There is good agreement with the limited experimental data. Due to these limited data, the monoclinic  $\text{ZrO}_2$  phase was included only as a line compound. The calculated tetragonal  $\text{ZrO}_2$ /(tetragonal  $\text{ZrO}_2$  + cubic  $\text{ZrO}_2$ )/cubic  $\text{ZrO}_2$  shows better agreement with experimental data than in the  $\text{Y}_2\text{O}_3\text{-ZrO}_2$  system, as shown in Figures 7 and 5, respectively.

The third binary needed for this study is the  $\text{Y}_2\text{O}_3\text{-Yb}_2\text{O}_3$  system. This was treated as an ideal solution, in accordance with the limited experimental data (44), which shows a continuous cubic solid solution at 1923 K.

Next the binaries were combined to form the  $\text{Y}_2\text{O}_3\text{-Yb}_2\text{O}_3\text{-ZrO}_2$  pseudo-ternary. Additional ternary interaction coefficients were included and given in Table VI. Calculated sections for 1473, 1673, and 1923 K are shown in Figures 8(a), (b), and (c), respectively. The intermediate line compound  $\text{Zr}_3(\text{Y,Yb})_4\text{O}_{12}$  shows the experimentally observed behavior (Figures 3(a-c)). The tetragonal  $\text{ZrO}_2$ , cubic  $\text{ZrO}_2$ , and cubic  $(\text{Y,Yb})_2\text{O}_3$  phases also show continuous solid solutions, as observed experimentally.

## Conclusions

Experimental data for the  $\text{Y}_2\text{O}_3\text{-ZrO}_2$ ,  $\text{Yb}_2\text{O}_3\text{-ZrO}_2$ , and  $\text{Y}_2\text{O}_3\text{-Yb}_2\text{O}_3\text{-ZrO}_2$  systems has been examined. For the  $\text{Y}_2\text{O}_3\text{-ZrO}_2$  pseudo-binary a good deal of phase boundary data are available, but only limited thermodynamic data. For the other systems, only limited phase boundary data is available. A Calphad-type database was developed for both pseudo-binaries and put together for the pseudo-ternary.

## Acknowledgement

Partial supported for ZKL by an NSF Career Award under grant DMR-9983532 is greatly appreciated. The work at NASA was supported by the Ultra Efficient Engine Technology (UEET) Program.

**References:**

1. N. Saunders and A. P. Miodownik, CALPAD Calculation of Phase Diagrams A Comprehensive Guide, Oxford, UK, Pergamon, 1998.
2. L. Kaufman, "Calculation of Multicomponent Ceramic Phase Diagrams," *Physica B* 150 99-114 (1988).
3. S. A. Degtyarev and G. F. Voronin, "Solution of Incorrect Problems in the Thermodynamics of Phase Equilibria. I. The System  $ZrO_2$ - $Y_2O_3$ ," *Russ. J. Phys. Chem.* 61 [3], 317-20 (1987).
4. S. A. Degtyarev and G. F. Voronin, "Solution of "Incorrect" Problems in the Thermodynamics of Phase Equilibria. II. Calculation of the  $ZrO_2$ - $Y_2O_3$  Phase Diagram," *Russ. J. Phys. Chem.* 61 [3], 320-23 (1987).
5. Y. Du, Z. Jin, and P. Huang, "Thermodynamic Assessment of the  $ZrO_2$ - $YO_{1.5}$  System," *J. Am. Ceram. Soc.* 74 [7] 1569-77 (1991).
6. Y. Du, Z. Jin, and P. Huang, "Thermodynamic Calculation of the  $ZrO_2$ - $YO_{1.5}$ -MgO System," *J. Am. Ceram. Soc.* 74 [9] 2107-12 (1993).
7. H. L. Lukas, E.-Th. Henig, and B. Zimmermann, "Optimization of Phase Diagrams by a Least Squares Method Using Simultaneously Different Types of Data," *CALPHAD I* [3], 2215-36 (1977).
8. H. Yokokawa, N. Sakai, T. Kawada, and M. Dokiya, "Phase Diagram Calculations for  $ZrO_2$  Based Ceramics: Thermodynamic Regularities in Zirconate Formation and Solubilities of Transition Metal Oxides," *Science and Technology of Zirconia V*, ed. by S. P. S. Badwal, M. J. Bannister, and R. H. J. Hannink, Technomic, Lancaster, PA, 1993, pp. 59-68.
9. H. Yokokawa, "Phase Diagrams and Thermodynamic Properties of Zirconia Based Ceramics," *Key Engineering Materials*, 153-154, 37-74 (1998).
10. A. Dinsdale, *The SGTE Substance Data File*, National Physical Laboratory, Teddington, UK, 1987.
11. L. V. Gurvich, V. S. Iorish, D. V. Chekhovskoi, and V. S. Yungman, *IVTANTHERMO-A Thermodynamic Database and Software System for the Personal Computer*, NIST Special Database 5, NIST, Gaithersburg, MD, 1993.
12. V. S. Stubican, R. C. Hink, and S. P. Ray, "Phase Equilibria and Ordering in the System  $ZrO_2$ - $Y_2O_3$ ," *J. Am. Ceram. Soc.* 61 [1/2], 17-21 (1978).

13. O. Kubachewski and C. B. Alcock, Metallurgical Thermochemistry, Pergamon Press, Oxford, England, 1983.
14. M. A. Clevinger, K. M. Hill, T. R. Green, C. C. Cedeno, E. Hayward, and N. Swanson, "Phase Equilibrium Diagrams, CD-ROM Database, Version 2.1," Am. Ceram. Soc., Westerville, OH, 1993, Figure 93-023.
15. *ibid.*, Figure 93-055.
16. P. Duwez, F. H. Brown, Jr., and Odell, F., "The Zirconia-Yttria System," J. Electrochem. Soc. 98, 356-62 (1951).
17. T. Noguchi, M. Mizuno, and T. Yamada, "The Liquidus Curve of the  $ZrO_2$ - $Y_2O_3$  System as Measured by a Solar Furnace," Bull. Chem. Soc. Japan 43, 2614-16 (1970).
18. A. Rouanet, "Zirconium Dioxide-Lanthanide Oxide Systems Close to the Melting Point," Rev. Int. Hautes Temp. Refract. 8 [2], 161-80 (1971).
19. S. R. Skaggs, "The Zirconia-Yttria System above 2000°C," PhD Dissertation, University of New Mexico, Albuquerque, New Mexico, 1972.
20. K. K. Srivastava, R. N. Patil, C. B. Choudhary, K. V. G. K. Gokhale, and E. C. Subbaro, "Revised Phase Diagram of the System  $ZrO_2$ - $YO_{1.5}$ ," Trans. J. Brit. Ceram. Soc. 73 [2] 85-91 (1974).
21. H. G. Scott, "Phase relationships in the zirconia-yttria system," J. Mat. Sci. 10, 1527-35 (1975).
22. V. S. Stubican and J. R. Hellman, "Phase Equilibria in some zirconia systems," in Science and Technology of Zirconia, pp. 25-36, Advances in Ceramics, Volume 3, ed. by A. H. Heuer and L. W. Hobbs, American Ceramic Society, Columbus, OH, 1981.
23. V. Lanteri, A. H. Heuer, and T. E. Mitchell, "Tetragonal Phase in the System  $ZrO_2$ - $Y_2O_3$ ," Advances in Ceramics, Vol. 12, Science and Technology of Zirconia II, edited by N. Claussen, M. Rühle, and A. H. Heuer, Am. Ceram. Soc., Columbus, OH, 1983, pp. 118-30.
24. C. Pascual and P. Duran, "Subsolidus Phase Equilibria and Ordering in the System  $ZrO_2$ - $Y_2O_3$ ," J. Am. Ceram. Soc. 66 [1], 23-27 (1983).
25. M. Rühle, N. Claussen, and A. H. Heuer, "Microstructural Studies of  $Y_2O_3$ -Containing Tetragonal  $ZrO_2$  Polycrystals (Y-TZP)," pp. 325-370 Advances in Ceramics, Volume 12, ed. by N. Claussen, M. Rühle, and A. H. Heuer, American Ceramic Society, Columbus, OH, 1983.

26. G. S. Corman, "Phase Equilibria, Defect Ordering, and Ionic Conductivity in the Zirconia-Ytterbia-Yttria System," PhD Thesis, Pennsylvania State University, 1984.
27. R. Ruh, K. S. Mazdidasni, P. G. Valentine, and H. O. Bielstein, "Phase Relations in the System  $ZrO_2$ - $Y_2O_3$  at Low  $Y_2O_3$  Contents," *J. Am. Ceram. Soc.* C-190-92 (1984).
28. S. Stubican, G. S. Corman, J. R. Hellman, and G. Senft, "Phase Relationships in Some  $ZrO_2$  Systems," pp. 96-106, *Science and Technology of Zirconia II*, *Adv. in Ceramics*, Vol. 12, ed. by N. Claussen, M. Ruhle, and A. H. Heuer, Am. Ceram. Soc., Columbus, OH, 1984.
29. G. S. Corman and V. S. Stubican, "Phase Equilibria and Ionic Conductivity in the System-  $ZrO_2$ - $Yb_2O_3$ - $Y_2O_3$ ," *J. Am. Ceram. Soc.* 68 [4], 174-81 (1985).
30. N. Yoshikawa, H. Eda, and H. Suto, "On the Cubic/Tetragonal Phase Equilibrium of the  $ZrO_2$ - $Y_2O_3$  System," *J. Japan Inst. Metals* 50 [1], 113-18 (1986).
31. N. Yoshikawa and H. Suto, "Transformation Behavior of  $Y_2O_3$ -PSZ Investigated by Thermal Dilatometry," *J. Japan Inst. Metals* 50 [1], 108-13 (1986).
32. M. Yoshimura, "Phase Stability of Zirconia," *Am. Ceram. Soc. Bull.* 67 [12], 1950-55 (1988).
33. K. S. Mazdidasni, C. T. Lynch, and J. S. Smith II, "Cubic Stabilization of Translucent Yttria-Zirconia at Very Low Temperatures," *J. Am. Ceram. Soc.* 50 [10], 532-37 (1967).
34. D. K. Smith, "The Nonexistence of Yttrium Zirconate," *J. Am. Ceram. Soc.* 49 [11], 625-26 (1966).
35. V. S. Stubican, "Phase Equilibria and Metastabilities in the Systems  $ZrO_2$ - $MgO$ ,  $ZrO_2$ - $CaO$ , and  $ZrO_2$ - $Y_2O_3$ ," in *Science and Technology of Zirconia III*, edited by S. Sōmiya, N. Yamamoto, and H. Yanagida, Columbus, OH, 1986, pp. 71-82.
36. M. Jayaratna, M. Yoshimura, and S. Sōmiya, "Subsolidus Phase Relations in the Pseudoternary System  $ZrO_2$ - $YO_{1.5}$ - $CrO_{1.5}$ ," *J. Am. Ceram. Soc.* 67 [11], C-240-42 (1984).
37. T-S. Sheu, T-Y. Tien, and I-W. Chen, "Cubic-to-Tetragonal ( $t'$ ) Transformation in Zirconia-Containing Systems," *J. Am. Ceram. Soc.* 75 [5], 1108-16 (1992).
38. D-J. Kim, H-J. Jung, and I-S. Yang, "Raman Spectroscopy of Tetragonal Zirconia Solid Solutions," *J. Am. Ceram. Soc.* 76 [8], 2106-108 (1993).
39. A. N. Belov and G. A. Semenov, "Thermodynamics of Binary Solid Solutions of Zirconium, Hafnium, and Yttrium Oxides from High-temperature Mass Spectrometry Data," *Russ. J. Phys. Chem.* 59 [3], 342-44 (1985).

40. V. R. Korneev, V. B. Glushkova, and É. K. Keler, "Heats of Formation of Rare Earth Zirconates," *Izv. Akad. Nauk. Neorg. Mat.* 7, 781-82 (1971).
41. A. Bogicevic, C. Wolverton, G. M. Crosbie, and E. B. Stechel, "Defect ordering in aliovalently doped cubic zirconia from first principles," *Phys. Rev. B* 64, 014106-1-14 (2001).
42. O. Redlich, A. T. Kister, and C. E. Turnquist, "Thermodynamics of Solutions," *Chem. Eng. Progress, Symp. Series*, 48, 49-64 (1952).
43. Y. M. Muggianu, M. Gambino, J. P. Bros, "Enthalpies de Formation des Alliages Liquides Bismuth-Étain-Gallium a 723 K. Choix d'une Représentation Analytique des Grandeurs D'Excès Intégrales et Partielles de Mélange," *J. Chim. Physique et Pysico-Chim. Biol.* 72, 83-88 (1975).
44. *op. cit.* Clevinger, Figure 347.

Phase Transition	Temperature of transition (K)	$\Delta_{trans}H$ (kJ/mol)	Reference
ZrO <sub>2</sub> monoclinic → tetragonal	1445	8400	(11)
ZrO <sub>2</sub> tetragonal → cubic	2620	21400	(11)
ZrO <sub>2</sub> cubic → liquid	2983	111400	(11)
Y <sub>2</sub> O <sub>3</sub> cubic → hexagonal	2550 2599	54000 20000	(11) (12)*
Y <sub>2</sub> O <sub>3</sub> hexagonal → liquid	2712 2782	115000 114000	(11) (12)*
Yb <sub>2</sub> O <sub>3</sub> solid → liquid	2789	130000	(11)
Yb <sub>2</sub> O <sub>3</sub> cubic → hexagonal	2663	20000	(11)**
Yb <sub>2</sub> O <sub>3</sub> hexagonal → liquid	2703	12000	(11)**

\*Values from reference 11 modified to give agreement with data of reference 12.

\*\*Transition temperatures from reference 11 and heats are estimated.

Table I(a). Temperatures and enthalpies of transitions to define lattice stabilities.

Phase	Abbreviation	Temperature Range (K)	Gibbs energy (J/mol)
ZrO <sub>2</sub> --monoclinic	mz	298-1445	$-1125582.53+417.508432*T-68.32783*T*LN(T)-.0045415885*T**2+1.72444167E-10*T**3+671863.5*T**(-1)$
		1445-2620	$1129291.49+484.935707*T-78.1*T*LN(T)-1.0845475E-16*T**2+7.81505167E-21*T**3-7.622945E-08*T**(-1)$
		2620-2983	$-1134269.49+501.790474*T-80*T*LN(T)-2.0126725E-14*T**2+9.19196667E-19*T**3-5.127845E-05*T**(-1)$
		2983-6000	$-1193929.49+681.804169*T-100*T*LN(T)+3.041038E-16*T**2-8.75008833E-21*T**3+2.46697E-06*T**(-1)$
ZrO <sub>2</sub> --tetragonal	tz	298-6000	$G_{mz}(T) + 8400-5.81314879*T$
ZrO <sub>2</sub> --cubic	cz	298-6000	$G_{mz}(T)+21400-10.7749809*T$
ZrO <sub>2</sub> --liquid	Lz	298-6000	$G_{mz}(T)+111400-40.9459497*T$
ZrO <sub>2</sub> --cubic Y <sub>2</sub> O <sub>3</sub> phase	czy	298-6000	$G_{mz}(T)+21500$
ZrO <sub>2</sub> --hexagonal	hz	298-6000	$G_{mz}(T)+22500$
Y <sub>2</sub> O <sub>3</sub> --cubic	cy	298-1100	$2.98140E+02 -1945493.95+680.542373*T-113.9721*T*LN(T)-.012761235*T**2+1.49941783E-06*T**3+813690.5*T**(-1)$
		1100-2100	$-2012427.83+1275.75211*T-98.0735*T*LN(T)+.03498891*T**2-3.688465E-06*T**3+10928115*T**(-1)$
		2100-2599	$-2274854.51+2766.12583*T-94.0992*T*LN(T)+.10031335*T**2-7.78301833E-06*T**3+77093000*T**(-1)$
		2599-2782	$-2011617.72+1043.70289*T-160*T*LN(T)-5.08929E-13*T**2+2.42719833E-17*T**3-.00114311*T**(-1)$
		2782-6000	$-2120097.72+1399.92055*T-200*T*LN(T)+4.6124375E-16*T**2-1.38251267E-20*T**3+3.154309E-06*T**(-1)$
Y <sub>2</sub> O <sub>3</sub> --hexagonal	hy	298-6000	$G_{cy}(T)+20000-7.69527*T$
Y <sub>2</sub> O <sub>3</sub> --liquid	Ly	298-6000	$G_{cy}(T)+134000-48.67307*T$
Y <sub>2</sub> O <sub>3</sub> --monoclinic	my	298-6000	$G_{cy}(T)+22100$
Y <sub>2</sub> O <sub>3</sub> --tetragonal	ty	298-6000	$G_{cy}(T)+21100$
Y <sub>2</sub> O <sub>3</sub> --cubic ZrO <sub>2</sub> phase	cyz	298-6000	$G_{cy}(T)+20100$
Yb <sub>2</sub> O <sub>3</sub> --cubic	cyb	298-2663	$-1858343.67+747.941586*T-130.1851*T*LN(T)-.0018969155*T**2-7.66497333E-12*T**3+709650*T**(-1)$
		2663-2798	$-1923755.38+1002.70962*T-160*T*LN(T)$
		2798-6000	$-2035675.38+1360.17602*T-200*T*LN(T)$
Yb <sub>2</sub> O <sub>3</sub> --hexagonal	hyb	298-6000	$G_{cyb}(T)+20000-7.510327*T$
Yb <sub>2</sub> O <sub>3</sub> --liquid	Lyb	298-6000	$G_{cyb}(T)+140000-51.823473*T$
Yb <sub>2</sub> O <sub>3</sub> --monoclinic	myb	298-6000	$G_{cyb}(T)+22100$
Yb <sub>2</sub> O <sub>3</sub> --tetragonal	tyb	298-6000	$G_{cyb}(T)+21100$
Yb <sub>2</sub> O <sub>3</sub> --cubic ZrO <sub>2</sub> phase	cyz	298-6000	$G_{cyb}(T)+20100$

Table I(b). Lattice stabilities.

Invariant	Temperature (K)	Composition $x(\text{Y}_2\text{O}_3)$	Reference	Comments
Eutectic $\text{liq} = \text{cz} + \text{cy}$	2688	0.817	(12)	
	2603	0.76	(18)	
	2646	0.825	(19)	
Peritectic $\text{cy} = \text{liq} + \text{hy}$	2720	0.778	(12)	Introduced, not measured
Eutectoid $\text{cz} = \text{delta y} + \text{cy}$	1650	0.435	(27)	
Eutectoid $\text{tz} = \text{mz} + \text{cz}$	838	0.039	(21)	Difficult to attain equilibria at this low temperature
Eutectoid $\text{cz} = \text{mz} + \text{delta y}$	< 673	0.20-0.30	(12)	Difficult to attain equilibria at this low temperature Approximate eutectoid discussed in (12)
Decomposition Temperature of delta y	1523	0.4	(12)	
	1655	0.4	(35)	
	1648	0.4	(24)	
Eutectic $\text{liq} = \text{cz} + \text{cyb}$	2691	0.85	(19)	
Decomposition of delta yb	1898	0.4	(29)	

Table II. Experimentally determined invariant points in the  $\text{Y}_2\text{O}_3\text{-ZrO}_2$  and  $\text{Yb}_2\text{O}_3\text{-ZrO}_2$  systems and decomposition temperatures of delta phase.

Compound	Temperature (K)	Method	$\Delta_f H^\circ$ (from oxides) — kJ/mol	$\Delta_f H^\circ$ (from elements) — kJ/mol	Reference
$\text{Y}_2\text{Zr}_2\text{O}_7$	298	Calorimetry	-47.7	-4185.4	(36)
$\text{Zr}_3\text{Y}_4\text{O}_{12}$	0	First Principles— Generalized Gradient Approximation	-20.9	-6454	(37)
$\text{Zr}_3\text{Y}_4\text{O}_{12}$	0	First Principles— Local-Density Approximation	-14.7	-6448	(37)

Table III. Enthalpies of formation of intermediate compound.

Phase	Parameter	Value (J/mol)
Liquid	${}^0\text{L}$	$98445 - 45.67\text{T}$
	${}^1\text{L}$	$95521 - 30.52\text{T}$
Cubic $\text{ZrO}_2$	${}^0\text{L}$	$-144364 + 24.60\text{T}$
	${}^1\text{L}$	$-180000 + 62.25\text{T}$
Tetragonal $\text{ZrO}_2$	${}^0\text{L}$	$-22324 - 32.95\text{T}$
	${}^1\text{L}$	$-240000 + 50\text{T}$
Monoclinic $\text{ZrO}_2$	${}^0\text{L}$	$-90000 - \text{T}$
Hexagonal $\text{Y}_2\text{O}_3$	${}^0\text{L}$	-18000
Cubic $\text{Y}_2\text{O}_3$	${}^0\text{L}$	$-30735 - 20.97\text{T}$
	${}^1\text{L}$	$99126 - 66.03\text{T}$
$\text{Zr}_3\text{Y}_4\text{O}_{12}$	$\text{A} + \text{BT}$	$-45966 + 11.28\text{T}$

Table IV. Interaction parameters for  $\text{Y}_2\text{O}_3\text{-ZrO}_2$  system.

Phase	Parameter	Value (J/mol)
Liquid	<sup>0</sup> L	18466 - 15.72T
	<sup>1</sup> L	-42812 + 26.53T
Cubic ZrO <sub>2</sub>	<sup>0</sup> L	-116088 + 12.67T
	<sup>1</sup> L	-296755 + 98.69T
Tetragonal ZrO <sub>2</sub>	<sup>0</sup> L	-22326 + 33.00T
	<sup>1</sup> L	-240024 + 50T
Monoclinic ZrO <sub>2</sub>	<sup>0</sup> L	-90000 - T
Hexagonal Yb <sub>2</sub> O <sub>3</sub>	<sup>0</sup> L	-18000
Cubic Yb <sub>2</sub> O <sub>3</sub>	<sup>0</sup> L	-30735 - 20.97T
	<sup>1</sup> L	125000 - 66.03T
Zr <sub>3</sub> Yb <sub>4</sub> O <sub>12</sub>	A + BT	-50064 + 11T

Table V. Interaction parameters for Yb<sub>2</sub>O<sub>3</sub>-ZrO<sub>2</sub> system.

Ternary Phase	L(Y <sub>2</sub> O <sub>3</sub> -Yb <sub>2</sub> O <sub>3</sub> -ZrO <sub>2</sub> ) (J/mol)
Tetragonal ZrO <sub>2</sub>	0
Cubic ZrO <sub>2</sub>	110000
Zr <sub>3</sub> (Y, Yb) <sub>4</sub> O <sub>12</sub>	-8000
Cubic (Y, Yb) <sub>2</sub> O <sub>3</sub>	-100000

Table VI. Ternary interaction parameters for Y<sub>2</sub>O<sub>3</sub>-Yb<sub>2</sub>O<sub>3</sub>-ZrO<sub>2</sub>

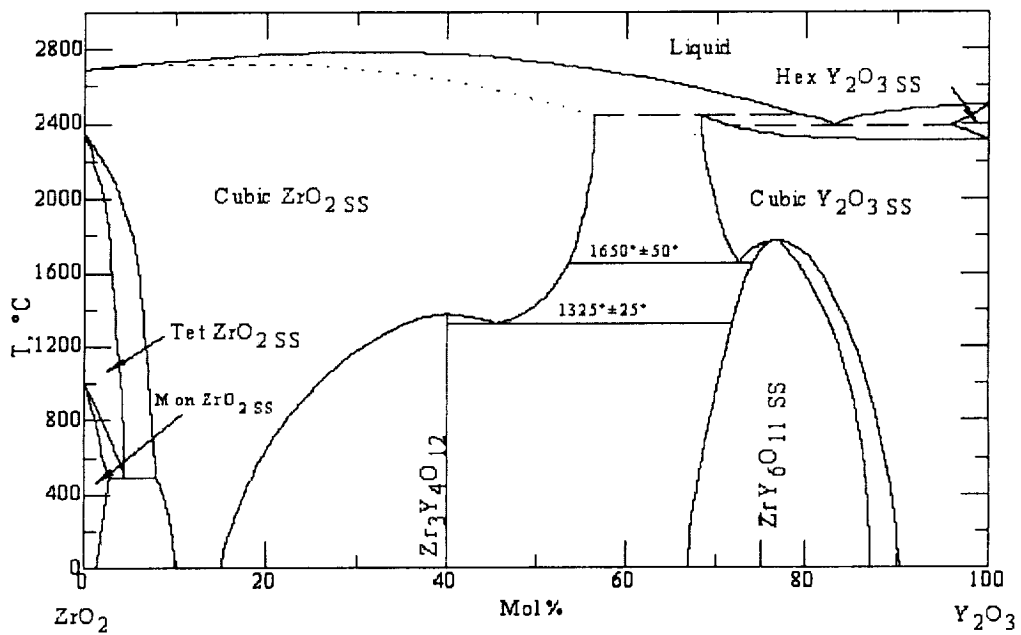
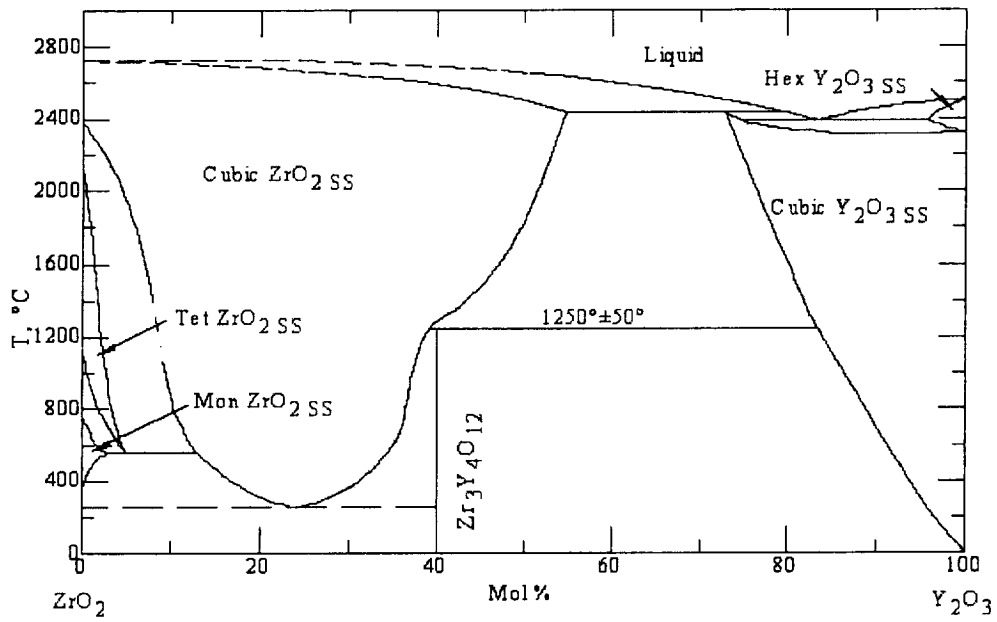


Figure 1. Accepted experimental phase diagrams for the  $\text{Y}_2\text{O}_3\text{-ZrO}_2$  system (14, 15).

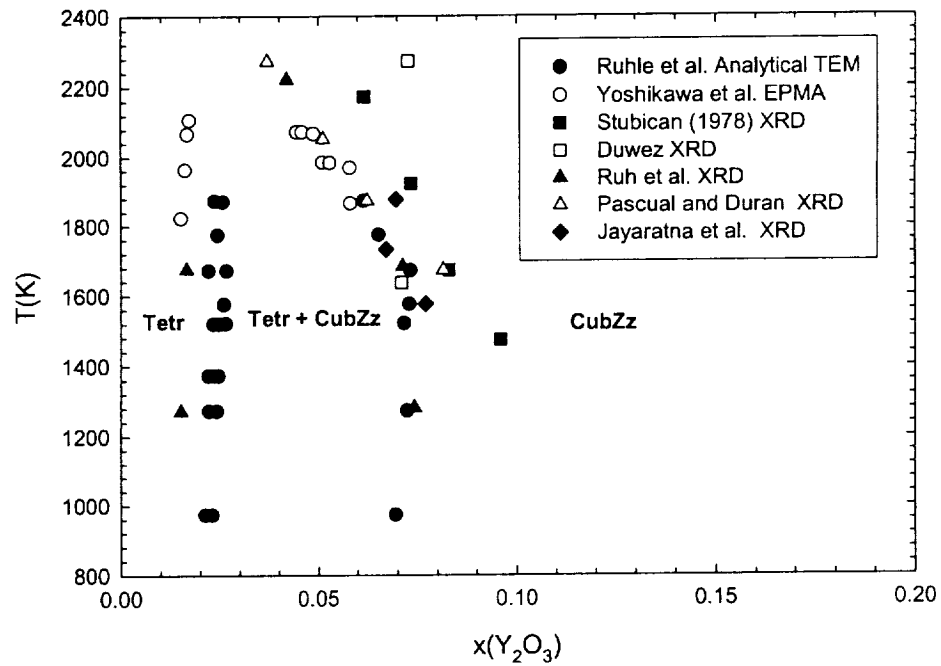


Figure 2—Experimental data for the tetragonal/(tetragonal + cubic)/cubic phase boundaries.

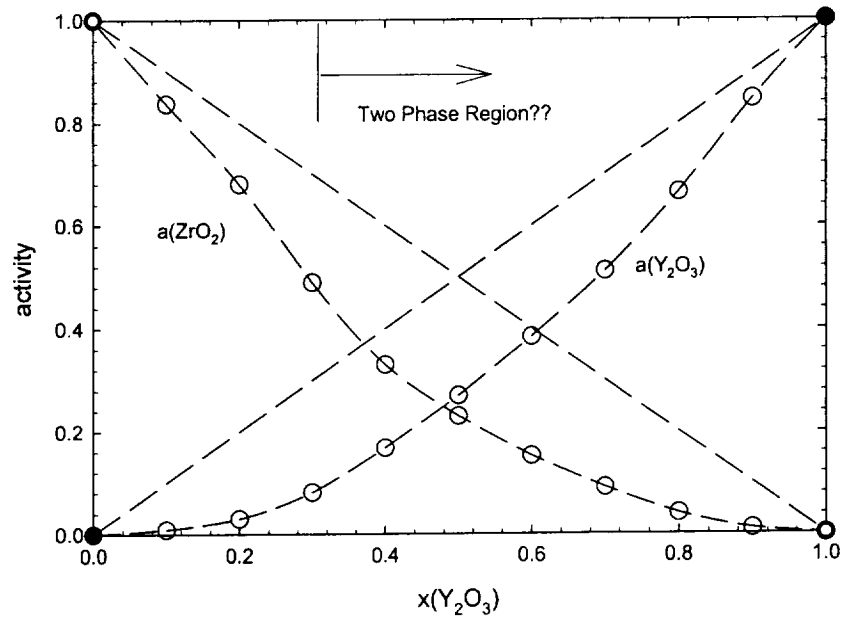


Figure 3. Activity of  $ZrO_2$  and  $Y_2O_3$  at 2773 K from Belov and Semenov (35)

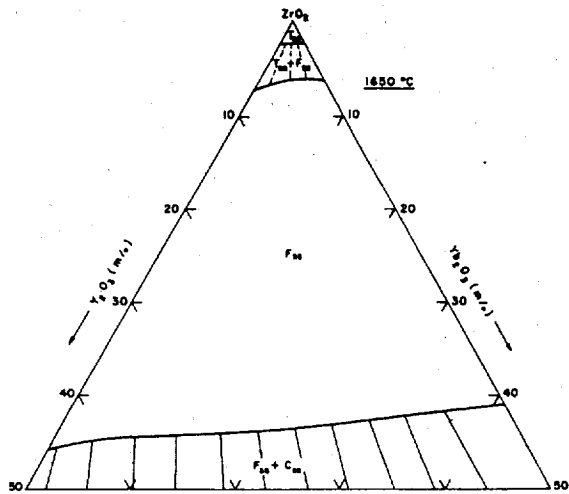
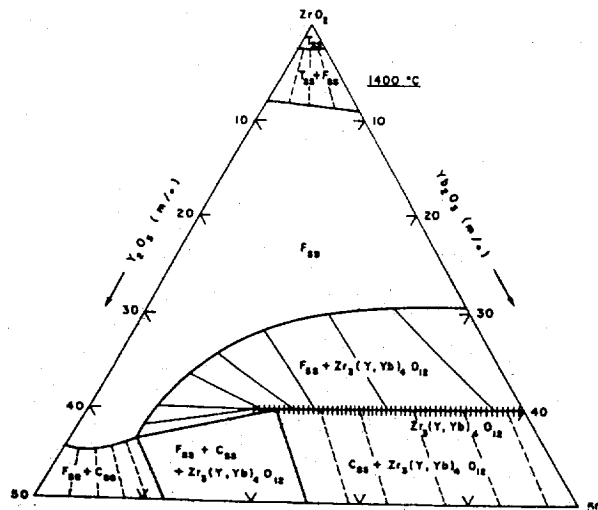
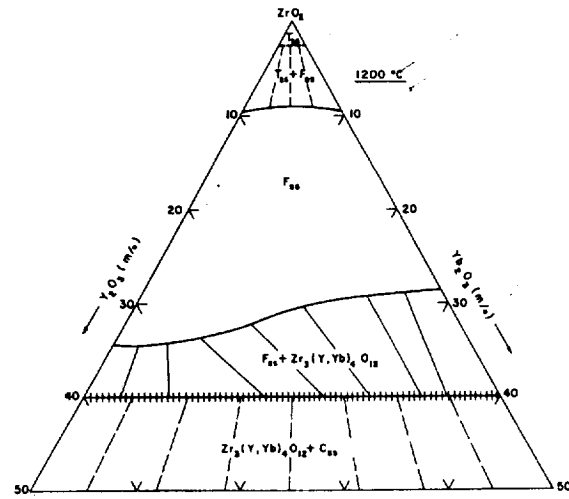


Figure 4. Experimental  $Y_2O_3$ - $Yb_2O_3$ - $ZrO_2$  ternary at (a) 1473 (b) 1673 (c) 1923 K (29).

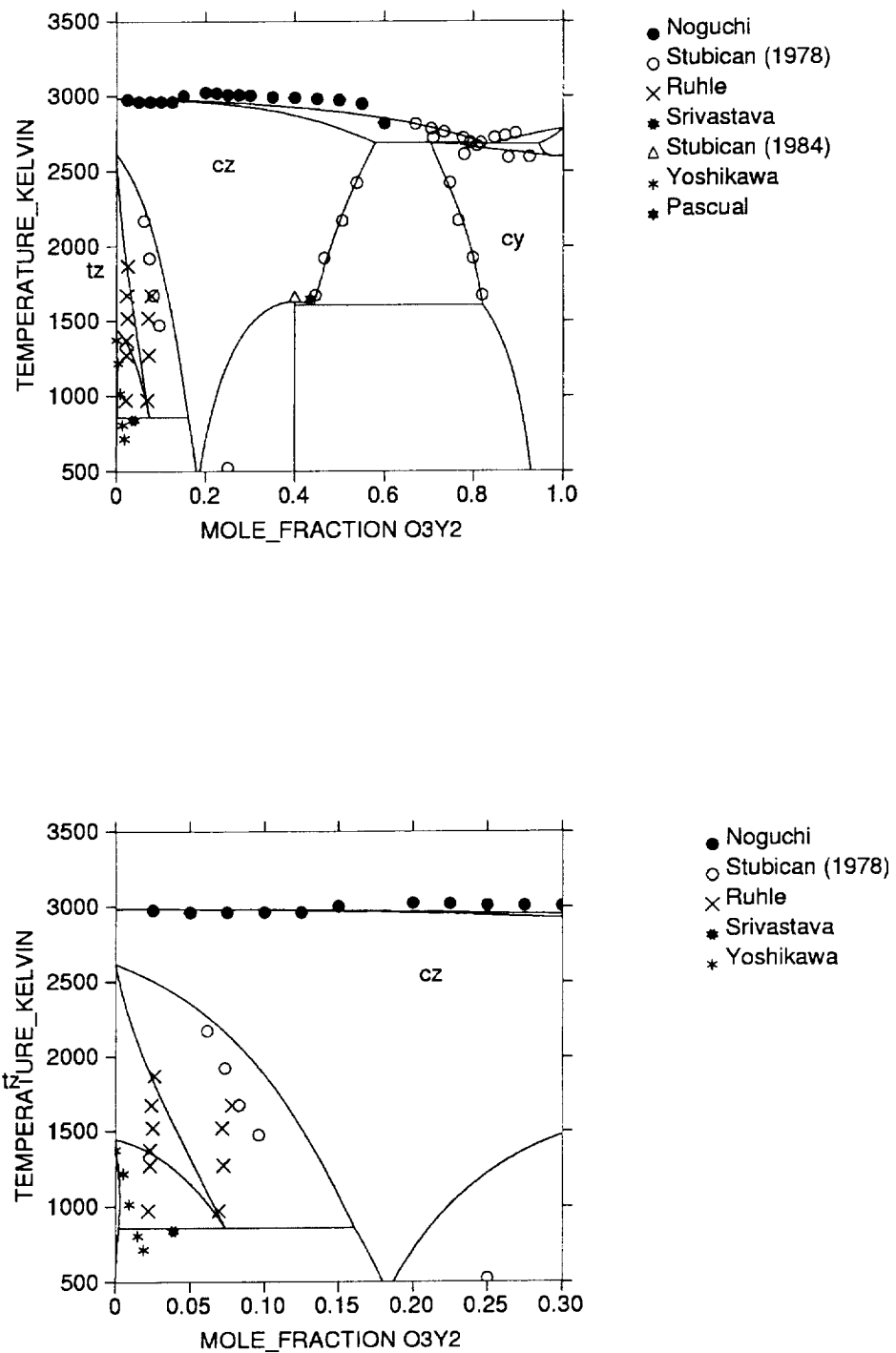


Figure 5. Calculated phase diagram for the  $Y_2O_3$ - $ZrO_2$  system. (a) Entire diagram (b) Enlargement of  $ZrO_2$ -rich region.

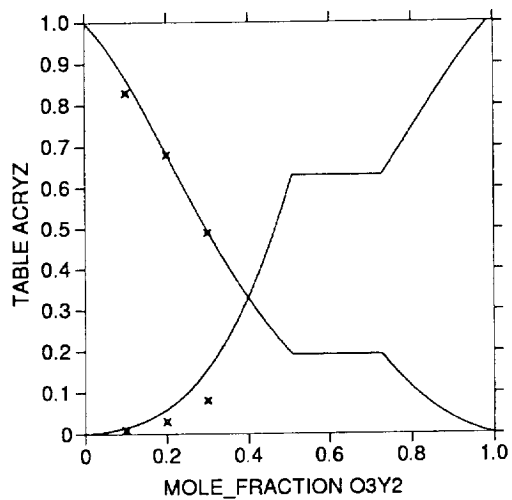


Figure 6. Plot of calculated activity in Y<sub>2</sub>O<sub>3</sub>-ZrO<sub>2</sub> system vs composition, showing experimental measurements (35).

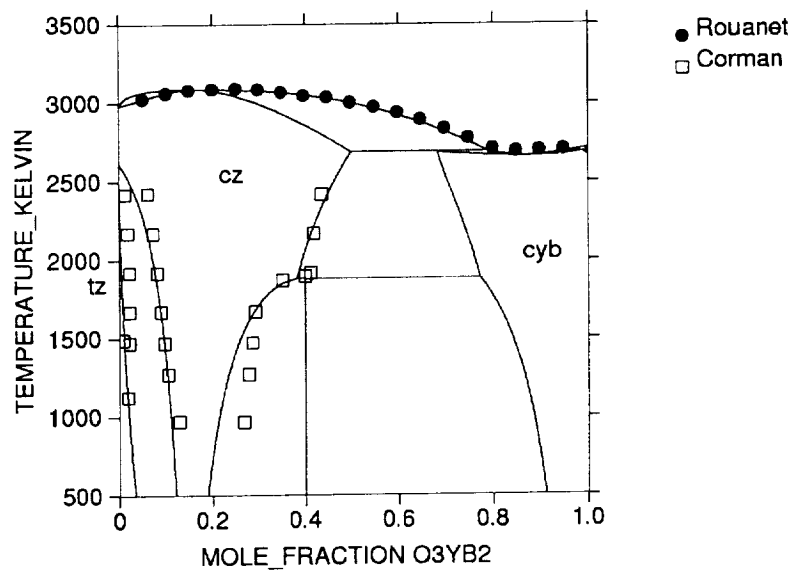
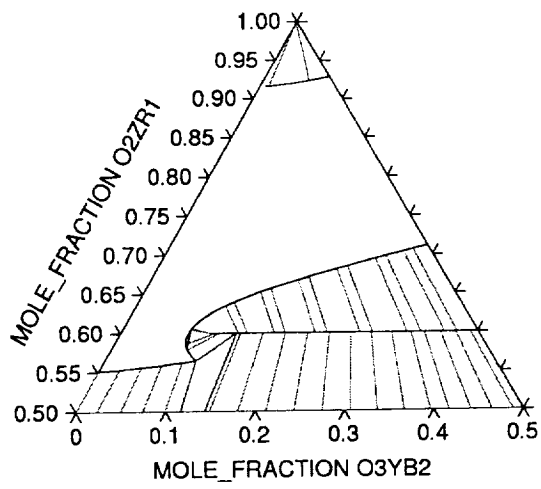
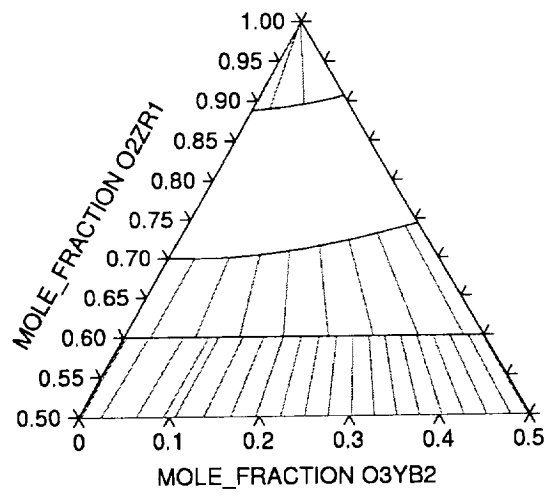


Figure 7. Calculated Yb<sub>2</sub>O<sub>3</sub>-ZrO<sub>2</sub> phase diagram.



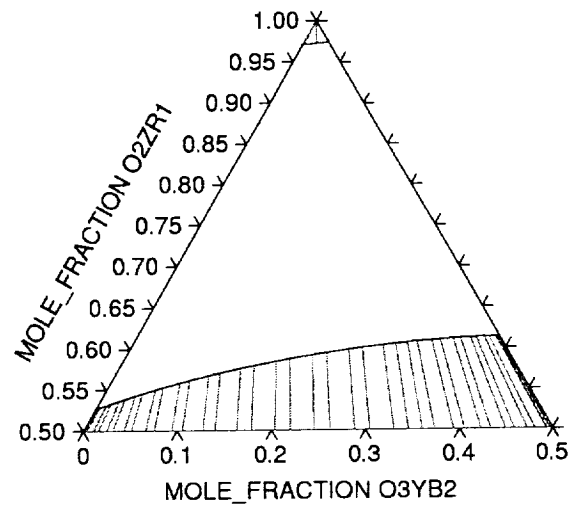


Figure 8. Calculated isothermal sections for  $\text{Y}_2\text{O}_3\text{-Yb}_2\text{O}_3\text{-ZrO}_2$  at (a) 1473 (b) 1673 and (c) 1923 K.